Published online 8 February 2019

Nucleic Acids Research, 2019, Vol. 47, No. 7 ***3395–3406***
doi: 10.1093/nar/gkz060

The E3-ligases SCF^{Ppa} and APC/C^{Cdh1} co-operate to regulate CENP-A^{CID} expression across the cell cycle

Olga Moreno-Moreno[1,2], Mònica Torras-Llort[1,2] and Fernando Azorin[1,2,*]

[1]Institute of Molecular Biology of Barcelona, IBMB, CSIC. Baldiri Reixac 4. 08028 Barcelona, Spain and [2]Institute for Research in Biomedicine, IRB Barcelona. The Barcelona Institute for Science and Technology. Baldiri Reixac 10, 08028 Barcelona, Spain

Received December 22, 2018; Revised January 22, 2019; Editorial Decision January 24, 2019; Accepted January 25, 2019

ABSTRACT

Centromere identity is determined by the specific deposition of CENP-A, a histone H3 variant localizing exclusively at centromeres. Increased CENP-A expression, which is a frequent event in cancer, causes mislocalization, ectopic kinetochore assembly and genomic instability. Proteolysis regulates CENP-A expression and prevents its misincorporation across chromatin. How proteolysis restricts CENP-A localization to centromeres is not well understood. Here we report that, in *Drosophila*, CENP-A^{CID} expression levels are regulated throughout the cell cycle by the combined action of SCF^{Ppa} and APC/C^{Cdh1}. We show that SCF^{Ppa} regulates CENP-A^{CID} expression in G1 and, importantly, in S-phase preventing its promiscuous incorporation across chromatin during replication. In G1, CENP-A^{CID} expression is also regulated by APC/C^{Cdh1}. We also show that Cal1, the specific chaperone that deposits CENP-A^{CID} at centromeres, protects CENP-A^{CID} from SCF^{Ppa}-mediated degradation but not from APC/C^{Cdh1}-mediated degradation. These results suggest that, whereas SCF^{Ppa} targets the fraction of CENP-A^{CID} that is not in complex with Cal1, APC/C^{Cdh1} mediates also degradation of the Cal1-CENP-A^{CID} complex and, thus, likely contributes to the regulation of centromeric CENP-A^{CID} deposition.

INTRODUCTION

Centromere identity is determined epigenetically by the specific deposition at centromeres of the histone H3 variant CENP-A (also called CenH3) (reviewed in (1–6)). Several mechanisms ensure that CENP-A is deposited only at centromeres. Centromeric CENP-A deposition is replication-independent (7,8) and, in most studied cases, occurs in G1 (9–14). CENP-A deposition requires the contribution of licensing factors, such as M18BP1 that recognizes centromeric chromatin and modifies it for deposition (15–19), and specific CENP-A chaperones, such as Scm3 in yeasts (20–22), Cal1 in *Drosophila* (23–28) and HJURP in vertebrates (29–31). In mammals, Cdk1/2 phosphorylates M18BP1 and HJURP inhibiting CENP-A loading outside of G1 (32). These mechanisms are overcome when CENP-A is overexpressed in yeast, *Drosophila* and mammalian cells, leading to its misincorporation across chromatin (33–42). In mammalian cells, ectopic CENP-A deposition depends on the H3.3 chaperone DAXX (43). Mistargeting of CENP-A to non-centromeric sites has important consequences since it leads to ectopic kinetochore formation, chromosome instability and aneuploidy (37,44–46). In this regard, increased CENP-A expression has been reported in several tumors, correlating with high aggressiveness and invasiveness (44,47–52). Therefore, it is of great importance to better understand the mechanisms that regulate CENP-A expression and stability.

Proteolytic degradation has been shown to regulate CENP-A expression in yeast and *Drosophila*, acting as a safeguard mechanism that prevents CENP-A misincorporation across chromatin (35,38). In yeast, four different E3-ubiquitin ligases have been reported to be involved in CENP-A^{Cse4} degradation (53–56). In *Drosophila*, the F-box protein Partner-of-paired (Ppa), which is a variable subunit of the E3-ubiquitin ligase SCF, has been shown to interact with CENP-A^{CID} and down-regulate its expression, preventing its ectopic deposition at non-centromeric sites (57). However, how these proteolytic activities regulate CENP-A stability across the cell cycle and contribute to its timely deposition at centromeres remains largely unknown. Here we analyze these questions *in vivo* in *Drosophila* and identify APC/C^{Cdh1} as a second major E3-ubiquitin ligase that, together with SCF^{Ppa}, regulates CENP-A^{CID} stability during cell cycle progression.

*To whom correspondence should be addressed. Tel: +3493 4034958; Email: fambmc@ibmb.csic.es

MATERIALS AND METHODS

Antibodies

Rabbit polyclonal αCENP-A^{CID} is described in (38). Rabbit polyclonal αCal1 is a gift from Dr Erhardt and is described in (73). The rest of antibodies used in these experiments are commercially available: mouse monoclonal αGFP (Roche, 11 814 460 001), rabbit polyclonal αActin (Sigma, A2066), rat monoclonal αElav (DSHB, 7E8A10), rabbit polyclonal αPH3 (Millipore, 06-570), mouse monoclonal αProspero (DSHB, MR1A) and mouse monoclonal αCut (DSHB, 2B10).

Stable S2 cell lines

ppa promoter (nucleotide position +1 to –1000) and *ppa* cDNA (the 3′UTR included) were obtained from genomic DNA by PCR-amplification using appropriate primers and cloned into pEGFP-C1 (Clontech) to generate plasmid pGFP-Ppa, which expresses GFP::Ppa under the control of the *ppa* promoter. To obtain stable cell lines, *Drosophila* S2 cells were grown under standard conditions (in Schneider's medium (Sigma) supplemented with 10% FBS (Gibco), 100 mg/ml Streptomycin and 100 mg/ml Penicillin at 25°C) and transfected by the calcium phosphate method (74) with pGFP-Ppa. After 48 h of transfection, 0.8 mg/ml G418 was added for selection.

Fly stocks and genetic procedures

Transgenic UAS-CENP-A^{CID}::YFP flies are described in (57). *ppa*^{RNAi} corresponds to line 9952R-2 from NIG-FLY and is described in (57). Transgenic UAS-Cal1 flies were kindly provided by Dr. Lehner and are described in (24). *APC2*^{RNAi}, *Cdh1*^{RNAi}, *Cdc20*^{RNAi} and *Cal1*^{RNAi} correspond to lines 106986, 25550, 40500 and 45248 from VDRC, respectively. *ey3.5*-GAL4, *longGMR*-GAL4 and *elav*-GAL4 were obtained from the Bloomington Stock Center. *ey3.5*-GAL4;UAS-CENP-A^{CID}::YFP and *longGMR*-GAL4;UAS-CENP-A^{CID}::YFP stocks were obtained by conventional genetic crosses and maintained at 18°C or 25°C.

For RNAi-mediated depletion experiments homozygous *ey3.5*-GAL4;UAS-CENP-A^{CID}::YFP and *longGMR*-GAL4;UAS-CENP-A^{CID}::YFP flies were crossed at 29°C to the corresponding homozygous RNAi flies and to *white* flies as control, except for *APC2*^{RNAi} where crosses were performed at 25°C. After 3 days adult flies were removed and the crosses were kept at the corresponding temperature until larvae reached the third-instar stage (∼5–6 days at 29°C and 7–8 days at 25°C). When the effects of *APC2*^{RNAi} and *APC10*^{RNAi} on endogenous CENP-A^{CID} expression levels were determined in third-instar larvae brains, depletion was induced by *elav*-GAL4 at 29°C. For Cal1 overexpression in *ppa*^{RNAi} or *Cdh1*^{RNAi} flies, homozygous *ppa*^{RNAi};UAS-Cal1 and *Cdh1*^{RNAi};UAS-Cal1 stocks were obtained by conventional genetic crosses and maintained at 18°C or 25°C. To analyze the effect on CENP-A^{CID}::YFP expression these lines were crossed at 29°C with homozygous *ey3.5*-GAL4;UAS-CENP-A^{CID}::YFP flies. After three days adult flies were removed and the crosses were kept at 29°C until larvae reached the third-instar stage (∼5–6 days).

Measure of eye size

When eye area was measured, adult flies were collected and kept at –20°C for 24 h. Images were collected using a SZX16 stereomicroscope equipped with an Olympus XC50 camera and CellD software. Eye images were measured and analyzed using Fiji software (75).

Fluorescence microscopy analysis

For direct fluorescence visualization, eye imaginal discs and salivary glands from third-instar larvae were dissected in PBS, fixed in 4% paraformaldehyde for 20 min at room temperature, washed in PBS/0.3% Triton X-100 three times for 10 min and once in PBS for 10 min, incubated for 30 min at room temperature with 0.02ng/μl DAPI in PBS, washed for 5 min in PBS/0.3% Triton X-100 and mounted in Mowiol (Calbiochem-Novabiochem). For immunostaining, eye imaginal discs were dissected and fixed as described above, washed in PBS/0.3% Triton X-100 three times for 10 min and blocked in PBS/0.3% Triton X-100/2% BSA three times for 10 min. Then, discs were incubated overnight at 4°C with the primary antibody diluted in blocking buffer, washed in blocking buffer three times for 10 min, incubated for 2 h at room temperature with secondary antibody in blocking buffer, washed in PBS/0.3% Triton X- 100 three times for 10 min and once in PBS for 10 min, incubated for 30 min at room temperature with 0.02 ng/μl DAPI in PBS, washed for 5 min in PBS/0.3% Triton X-100 and mounted in Mowiol (Calbiochem-Novabiochem). For immunostaining to detect endogenous CENP-A^{CID}, eye imaginal discs were processed as described above, but, after fixation, 0.25 M NaCl was added to the washes, the blocking and the incubation with the primary antibody. For larvae brains, squashes and immunostainings were performed as described in (57). In S2 cells, direct fluorescence microscopy visualization was performed with cells immobilized onto a slide by centrifugation for 10 min at 500 rpm on low acceleration in a TermoShandon Cytospin 4 using a single-chamber Cytospin funnel. Slides were fixed in 4% paraformaldehyde for 10 min, washed with PBS for 15 min and mounted in Mowiol (Calbiochem-Novabiochem). For immunolocalization with specific antibodies, cells were plated on cover slips treated with Concanavalin-A (Sigma) for 2 h at 25°C. Then they were washed with PBS for 10 min, fixed in 4% paraformaldehyde for 15 min, washed with PBS for 15 min, blocked in PBS/0.1% Triton X-100/0.1% BSA for 20 min and incubated with primary antibodies in blocking solution overnight at 4°C. After incubation, cover slips were washed three times for 10 min with blocking solution and incubated for 1 h at room temperature with secondary antibody diluted in blocking solution. Finally, they were washed twice for 10 min in PBS/0.1% Triton X-100, twice in PBS, and mounted in Mowiol (Calbiochem-Novabiochem) containing 0.2 ng/ml DAPI (Sigma). Primary antibodies were αElav (1:100), αPH3 (1:2000), αCENP-A^{CID} (1:300), αProspero (1:10) and αCut (1:100). Secondary antibodies were coupled to Cy3 and Cy5 (Jackson Immunore-

search laboratories) and were used at 1:400 dilutions. Images were collected in a Leica TCS/SPE confocal microscope equipped with LAS/AF software and analyzed with Fiji software (75). To determine nuclei size in salivary glands Fiji software was used to create a mask with DAPI channel and the area of each nucleus was determined. For quantitative analyses of endogenous CENP-A^{CID} levels in eye imaginal discs, fluorescence intensity was determined using the Fiji distribution of ImageJ (75). Integrated density of CENP-A^{CID} spots were calculated using a mask of CENP-A^{CID} channel created from thresholded images on the FeatureJ Laplacian (http://imagescience.org/meijering/software/featurej/) of the regions of interest (anterior or posterior to MF) and running Analyze particles plugin.

EdU incorporation

For EdU incorporation experiments, salivary glands from third-instar larvae were dissected in PBS and incubated with 10μM EdU (ThermoFisher Scientific) for 5 min at room temperature. EdU detection was performed with Click-iT™ Plus EdU Alexa Fluor™ 594 Imaging Kit (ThermoFisher Scientific) following manufacturer's protocol. DAPI staining, mounting and fluorescence visualization were performed as described above.

Western blot (WB) analysis

Total protein extracts were prepared from 35 third-instar larvae salivary glands dissected in PBS. Dissected salivary glands were transferred to 1xPLB/0.05% NP40/2mM PMSF, disrupted by pipetting and boiled 5 min at 95°. Extracts were analyzed by WB with αGFP (1:2000) (to detect the YFP signal), αCal1 (1:2000) and αActin (1:1000) antibodies. Quantitative analyses were carried out with a GS-800 Calibrated Densitometer (Bio-Rad) and Fiji software (75).

FACS sorting

For FACS sorting, cells were fixed in 1% paraformaldehyde for 1 h at 4°C, permeabilized with 70% ethanol and stained with 1 μg/ml DAPI (Sigma). Then, cells were sorted in an Aria SORP flow cytometer (Becton Dickinson) with a UV laser.

RESULTS

Ppa regulates CENP-A^{CID} expression in G1 and S-phase

Previous results showed that the E3-ligase SCF^{Ppa} regulates CENP-A^{CID} stability (57). In general, the activity of SCF complexes is cell cycle regulated (58–61). Thus, we analyzed the effect of SCF^{Ppa} on CENP-A^{CID} stability across the cell cycle. For this purpose, we took advantage of the cell cycle synchronization that the morphogenetic furrow (MF) induces in the eye imaginal disc of third instar larvae (62,63). MF is a dorso-ventral indentation that moves anterior and induces differentiation. Immediately anterior to MF, asynchronously dividing cells undergo a first synchronized mitosis (FMW). Later, exiting the MF, posterior cells undergo a second synchronized mitosis (SMW), arrest in G1 and differentiate (Figure 1A). In this experimental setting, we induced ectopic expression of a UAS-CENP-A^{CID}::YFP construct in G1-arrested cells using *ey3.5*-GAL4, which is active posterior to the MF (Supplementary Figure S1A, top). Under these conditions, we detected low CENP-A^{CID}::YFP expression (Figure 1B, top). However, simultaneous depletion of Ppa strongly increased CENP-A^{CID}::YFP levels in G1-arrested posterior cells (Figure 1B, bottom). This increase was not due to a defect on cell cycle progression and proliferation since Ppa depletion did not significantly affect the number of mitotic cells in the posterior region of eye imaginal discs (Figure 1C) or eye size in adult flies (Figure 1D).

We also analyzed the effect of Ppa depletion on CENP-A^{CID}::YFP expression in salivary glands, where *ey3.5*-GAL4 is also active (Supplementary Figure S1B). Salivary gland cells undergo multiple endoreplication cycles in which, after DNA replication, cells skip G2/M and reenter G1 (64–66). As in the eye imaginal disc, Ppa depletion increased CENP-A^{CID}::YFP levels, as determined by both immunofluorescence (IF) (Figure 2A) and western blot (WB) analyses (Figure 2B). EdU-incorporation experiments showed that CENP-A^{CID}::YFP levels increased in both EdU-negative G1 cells and replicating EdU-positive cells (Figure 2C). Ppa depletion did not significantly affect the proportion of EdU-positive cells (Figure 2D) or the number of nuclei per gland and their size (Figure 2E), suggesting that it did not significantly affect endocycling of salivary gland cells. These results confirm that Ppa regulates CENP-A^{CID} expression in G1 and that, at least in the specialized salivary glands cells, Ppa is also acting during chromatin replication in S-phase.

Next, we performed similar experiments using long*GMR*-GAL4 to induce UAS-CENP-A^{CID}::YFP expression in the eye imaginal disc cells located most posterior to the MF (Supplementary Figure S1A, bottom). Also in this case, CENP-A^{CID}::YFP levels were very low in control flies and increased upon Ppa depletion (Figure 3A). Concomitantly, a necrotic eye phenotype was observed in ∼60% of adult flies ($N = 33$) (Figure 3B). We observed that cells showing increased CENP-A^{CID}::YFP levels did not stain with markers of neuronal and cone cell differentiation (Figure 3C, top and Supplementary Figure S2), suggesting that they corresponded to cells that remain undifferentiated in the larval eye imaginal disc. As a matter of fact, secondary and tertiary pigment cells and mechanosensory bristles differentiate later at the pupae stage (62,63,67). These undifferentiated cells can eventually undergo mitosis. In this regard, we observed that cells showing increased CENP-A^{CID}::YFP levels were not stained with αPH3 (Figure 3C, bottom). Similar results were observed in experiments using *ey3.5*-GAL4. Also in this case, αPH3-positive posterior cells generally showed low CENP-A^{CID}::YFP levels (Figure 1E, left). In fact, upon Ppa depletion, cells showing high levels of mislocalized CENP-A^{CID}::YFP mainly corresponded to αPH3-negative cells (Figure 1E, right). Altogether these results suggest that Ppa is not regulating CENP-A^{CID}::YFP levels in mitosis. In this regard, it is possible that Ppa is not expressed or, alternatively, it is not active during mitosis. Specific αPpa

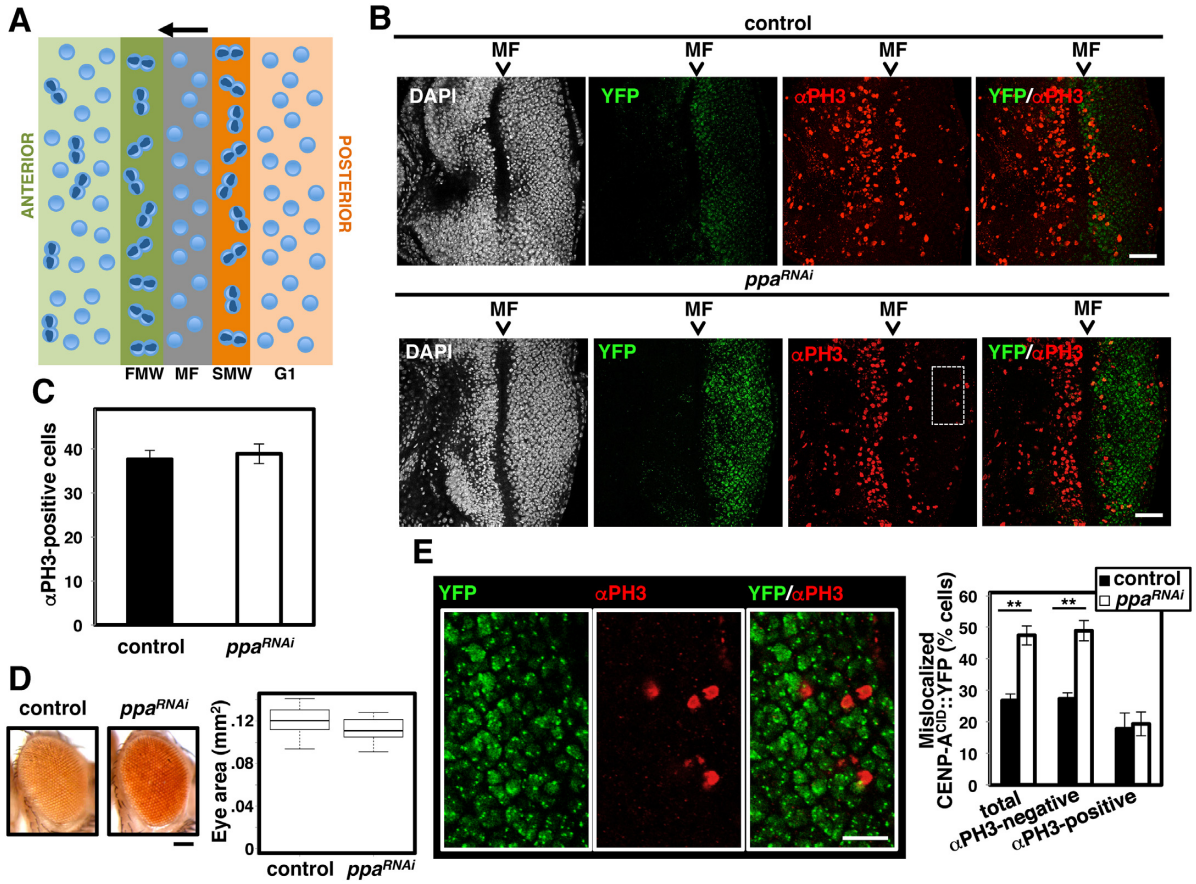

Figure 1. Ppa regulates CENP-A^{CID} expression in G1. (**A**) Schematic representation of the synchronization induced by the morphogenetic furrow (MF) in the eye imaginal disc. FMW, first mitotic wave. SMW, second mitotic wave. G1, G1-arrested cells. MF moves from posterior to anterior as indicated. (**B**) The expression of CENP-A^{CID}::YFP in the eye imaginal disc is determined by direct fluorescence (in green) in control *ey3.5*>CENP-A^{CID}::YFP flies (top) and upon Ppa depletion in *ey3.5*>CENP-A^{CID}::YFP; *ppa*^{RNAi} flies (bottom). Immunostainings with αPH3, which marks mitotic cells, are also presented (in red). DNA was stained with DAPI (in white). The position of the MF is indicated. Scale bar corresponds to 25 μm. (**C**) The number of posterior αPH3-positive cells per disc is presented for control *ey3.5*>CENP-A^{CID}::YFP flies ($N = 10$) and Ppa-depleted *ey3.5*>CENP-A^{CID}::YFP; *ppa*^{RNAi} flies ($N = 7$) (P-value > 0.01, two-tailed t-test; error bars are SEM). **D**) In the left, the eye phenotypes of control *ey3.5*>CENP-A^{CID}::YFP flies and Ppa-depleted *ey3.5*>CENP-A^{CID}::YFP; *ppa*^{RNAi} flies are presented. Scale bar corresponds to 100 μm. In the right, quantitative analysis of the results showing box plots of the eye area of control *ey3.5*>CENP-A^{CID}::YFP flies ($N = 20$) and Ppa-depleted *ey3.5*>CENP-A^{CID}::YFP; *ppa*^{RNAi} flies ($N = 20$). (P-value > 0.01, two-tailed t-test). (**E**) In the left, enlarged images of the region indicated by the box in A. Scale bar corresponds to 10 μm. In the right, the percentage of cells showing high levels of mislocalized CENP-A^{CID}::YFP in the posterior region of eye imaginal discs from control *ey3.5*>CENP-A^{CID}::YFP flies ($N = 7$) and Ppa-depleted *ey3.5*>CENP-A^{CID}::YFP; *ppa*^{RNAi} flies ($N = 5$) is presented for total and αPH3-negative and –positive cells (**P-value < 0.001, two-tailed t-test; errors bars are SEM).

antibodies that could be used to directly address this question are not available. However, using a stable S2 cell line expressing a GFP::Ppa tagged construct under the control of the *Ppa* promoter, we detected GFP::Ppa expression in αPH3-positive cells (Supplementary Figure S3A), as well as in G2/M FACS-sorted cells (Supplementary Figure S3B). GFP::Ppa expression was also detected in G1- and S-phase sorted cells (Supplementary Figure S3B). Altogether these results suggest that, although Ppa is apparently expressed throughout the cell cycle, its contribution to the regulation of CENP-A^{CID} stability is restricted to G1 and S-phase.

APC/C also regulates CENP-A^{CID} expression in G1

Results reported above indicate that the effects of Ppa depletion on CENP-A^{CID}::YFP expression are not uniform during cell cycle progression and differentiation. Yet, in those cell types and cell cycle phases where Ppa depletion caused no effect, CENP-A^{CID}::YFP levels remained low, suggesting that additional factors contribute to the regulation of CENP-A^{CID} stability. In this regard, we tested whether APC/C, a major cell cycle regulated E3-ligase (59–61,68), contributes to CENP-A^{CID} stability. We observed that depletion of APC2, an essential APC/C subunit, increased CENP-A^{CID}::YFP levels in salivary glands (Figure 4A and B), without affecting endocycling since it had no significant effects on the number of nuclei per gland and their size (Figure 4E). These results suggest that APC/C also regulates CENP-A^{CID} expression.

APC/C forms two main complexes, APC/C^{Cdc20} and APC/C^{Cdh1}, which are active at different cell cycle phases (59–61,68). APC/C^{Cdc20} is active during mitosis and promotes transition from metaphase to anaphase. At the exit from mitosis, Cdh1 replaces Cdc20 and APC/C^{Cdh1} remains active through G1, being degraded at the G1-to-S tran-

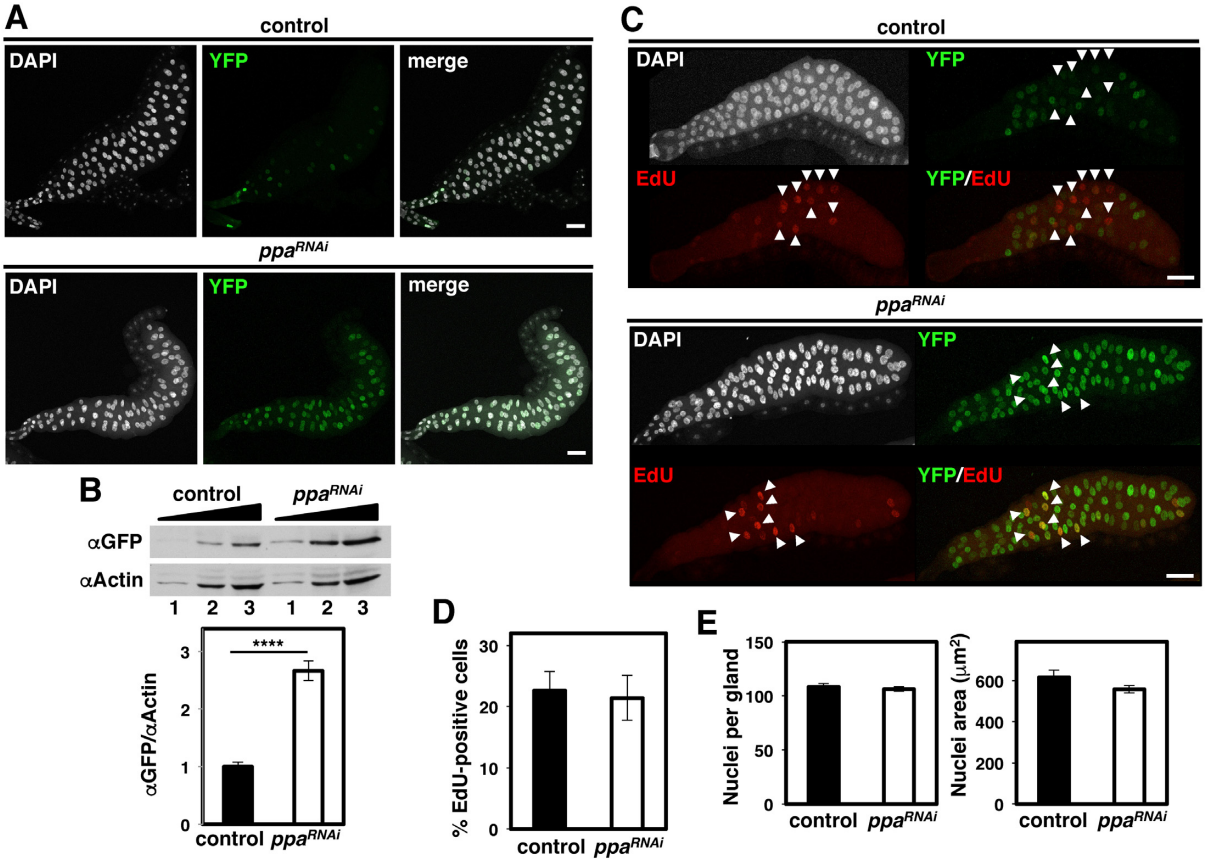

Figure 2. Ppa regulates CENP-A^{CID} expression during DNA replication. (**A**) The expression of CENP-A^{CID}::YFP in salivary glands is determined by direct fluorescence (in green) in control *ey3.5*>CENP-A^{CID}::YFP flies (top) and Ppa-depleted *ey3.5*>CENP-A^{CID}::YFP; *ppa^{RNAi}* flies (bottom). DNA was stained with DAPI (in white). Scale bars correspond to 100 μm. (**B**) Western blot (WB) analysis with αGFP antibodies of the levels of CENP-A^{CID}::YFP expression in salivary glands from control *ey3.5*>CENP-A^{CID}::YFP flies and Ppa-depleted *ey3.5*>CENP-A^{CID}::YFP; *ppa^{RNAi}* flies. Increasing amounts of extract are analyzed (lanes 1–3). αActin antibodies were used as loading control. Quantitative analysis of the results is shown in the bottom ($N = 3$; ****P-value < 0.00001, two-tailed t-test; errors bars are SEM). (**C**) As in A, but for salivary glands subjected to EdU-incorporation (in red) to detect replicating cells. Arrows indicate EdU-positive cells. Scale bars correspond to 100 μm. (**D**) The percentage of EdU-positive salivary gland cells is presented for control *ey3.5*>CENP-A^{CID}::YFP flies ($N = 8$) and Ppa-depleted *ey3.5*>CENP-A^{CID}::YFP; *ppa^{RNAi}* flies ($N = 12$) (P-value > 0.01, two-tailed t-test; error bars are SEM). (**E**) In the left, the number of nuclei per gland is presented for control *ey3.5*>CENP-A^{CID}::YFP flies ($N = 10$) and Ppa-depleted *ey3.5*>CENP-A^{CID}::YFP; *ppa^{RNAi}* flies ($N = 24$) (P-value > 0.01, two-tailed t-test; error bars are SEM). In the right, nuclei area of salivary glands cells is presented for control *ey3.5*>CENP-A^{CID}::YFP flies ($N = 10$) and Ppa-depleted *ey3.5*>CENP-A^{CID}::YFP; *ppa^{RNAi}* flies ($N = 24$) (P-value > 0.01, two-tailed t-test; error bars are SEM).

sition. Later, at the G2-to-M transition, Cdk1 phosphorylation activates APC/C^{Cdc20}. Next, we addressed which APC/C form regulates CENP-A^{CID}. We observed that Cdh1 depletion increased CENP-A^{CID}::YFP levels in salivary glands (Figure 4C and D), without significantly affecting endocycling (Figure 4E), which suggest that APC/C^{Cdh1} also regulates CENP-A^{CID} expression in G1. Cdc20 depletion also increased CENP-A^{CID}::YFP expression (Figure 4D), though to a lower extent than Cdh1 depletion. In fact, Cdc20 depletion is not expected to have strong effects in salivary glands since APC/C^{Cdc20} is mainly active in mitosis. In this regard, we observed that Cdc20 depletion in the eye imaginal disc increased CENP-A^{CID}::YFP expression too (Supplementary Figure S4A). Cdc20 depletion in cycling cells induces strong mitotic arrest and affects proliferation (69,70). Accordingly, in the eye imaginal disc, we observed strong proliferation defects and highly increased αPH3-reactivity upon Cdc20 depletion (Supplementary Figure S4A). Therefore, in this case, increased CENP-A^{CID}::YFP expression could be indirect through an effect on cell cycle progression. However, cells showing high levels of mislocalized CENP-A^{CID}::YFP were generally αPH3-negative (Supplementary Figure S4B, top), suggesting that they were not arrested in mitosis. In addition, the increment in the total number of αPH3-positive cells was mainly associated with cells showing no detectable CENP-A^{CID}::YFP mislocalization (Supplementary Figure S4B, bottom), suggesting that cells arrested in mitosis had low CENP-A^{CID}::YFP expression.

Next, we analyzed the contribution of APC/C^{Cdh1} to the regulation of endogenous CENP-A^{CID} expression. We observed that the intensity of immunostaining with αCENP-A^{CID} in the posterior region of the eye imaginal disc is lower than in the anterior region (Figure 5A). However, upon Cdh1 depletion, CENP-A^{CID} expression in the posterior compartment increased and equalized expression in the anterior region (Figure 5A). In addition, specific depletion of APC2 or APC10, another essential APC/C subunit, in

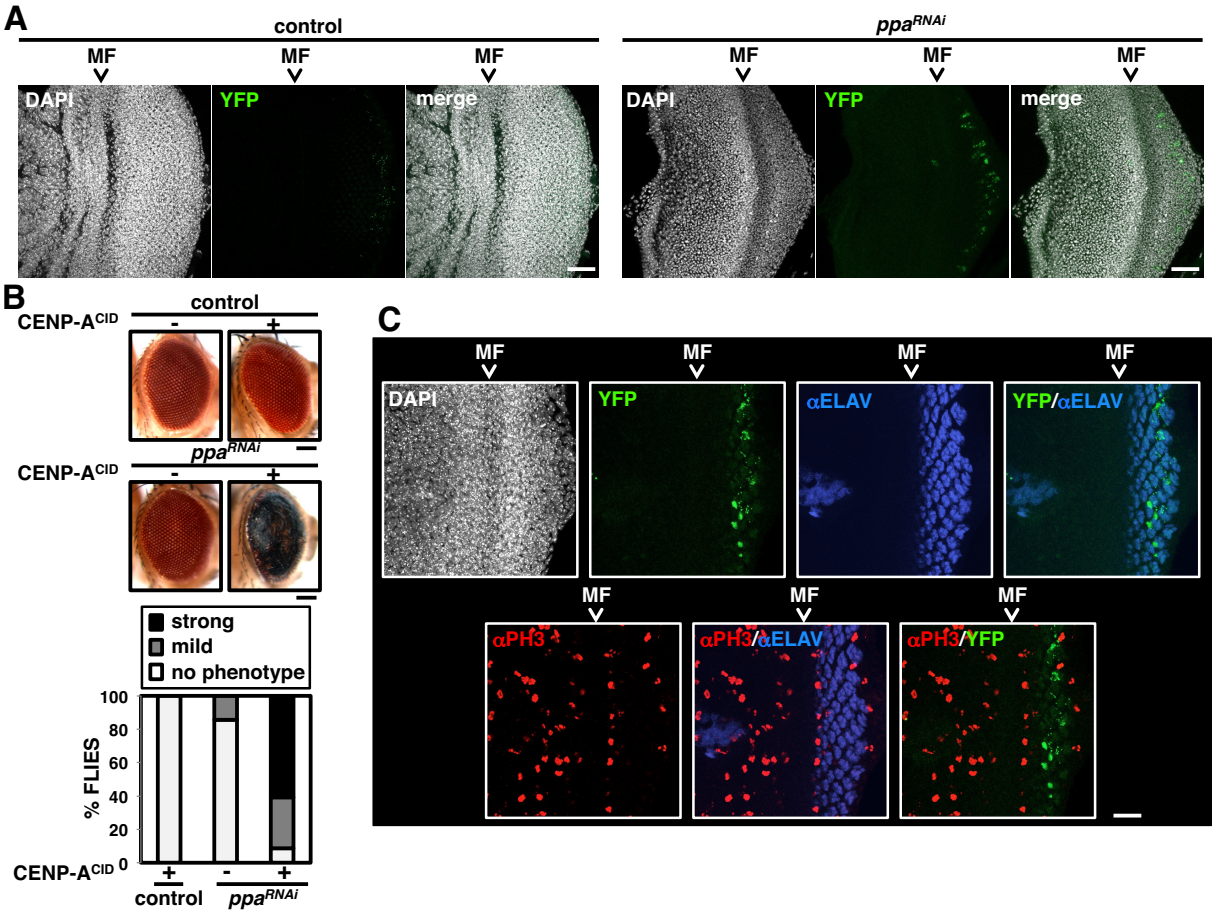

Figure 3. Ppa does not regulate CENP-A^{CID} expression in differentiated cells in the eye imaginal disc. (**A**) The expression of CENP-A^{CID}::YFP in the eye imaginal disc is determined by direct fluorescence (in green) in control *longGMR*>CENP-A^{CID}::YFP flies (left) and Ppa-depleted *longGMR*>CENP-A^{CID}::YFP; *ppa*^{RNAi} flies (right). DNA was stained with DAPI (in white). The position of the MF is indicated. Scale bars correspond to 25 μm. (**B**) The eye phenotypes of control long*GMR*-GAL4 flies and Ppa-depleted *longGMR*>*ppa*^{RNAi} flies, expressing CENP-A^{CID}::YFP (+) or not (–), are presented. Scale bars correspond to 100 μm. In the bottom, the proportions of flies showing strong, mild or no necrotic eye phenotype are presented for the indicated genotypes ($N > 56$). (**C**) Immunostaining with αELAV (in blue), which marks neuronal differentiated cells, and αPH3 (in red), which marks mitotic cells, of eye imaginal discs from Ppa-depleted *longGMR*>CENP-A^{CID}::YFP; *ppa*^{RNAi} flies. CENP-A^{CID}::YFP expression is determined by direct fluorescence (in green). DNA was stained with DAPI (in white). The position of the MF is indicated. Scale bar corresponds to 25 μm.

larvae brains using an *elav*-GAL4 driver also increased endogenous CENP-A^{CID} levels (Figure 5B). Altogether these results suggest that APC/C^{Cdh1} regulates expression of endogenous CENP-A^{CID}.

Cal1 protects CENP-A^{CID} from Ppa-mediated degradation, but not from Cdh1-mediated degradation

The interaction with Cal1 has been proposed to protect CENP-A^{CID} from proteolytic degradation (25,27). However, we observed that CENP-A^{CID}::YFP levels were not significantly affected upon Cal1 depletion (Figure 6A and B) or overexpression (Figure 6C and D), which is in contrast to previous results in S2 cells showing reduced endogenous CENP-A^{CID} levels upon Cal1 depletion (25,27). To address this apparent contradiction we analyzed the contribution of Cal1 to Ppa- and Cdh1-mediated degradation separately. We observed that Cal1 protected CENP-A^{CID}::YFP from Ppa-mediated degradation since in salivary glands from Cdh1-knockdown larvae, where Ppa principally mediates CENP-A^{CID}::YFP degradation, Cal1 depletion reduced CENP-A^{CID}::YFP levels (Figure 7A and B). Moreover, upon Cal1 overexpression in Cdh1-knockdown glands, IF experiments showed a marked increase of CENP-A^{CID}::YFP levels in ∼30% of the glands ($N = 21$) (Figure 7D, gland in the right of panel Cdh1^{RNAi}; >Cal1). A similar tendency to increase was detected in WB analyses (Figure 7C). On the contrary, in Ppa-knockdown glands, WB analyses showed that Cal1 depletion did not significantly affect CENP-A^{CID}::YFP levels (Figure 7E and F), suggesting that Cal1 did not protect CENP-A^{CID}::YFP from Cdh1-mediated degradation. Moreover, upon Cal1 overexpression, although global CENP-A^{CID}::YFP levels were not affected (Figure 7G), we observed a marked reduction in the number of YFP-positive cells (Figure 7H). This reduction was accompanied by a change in the pattern of localization of CENP-A^{CID}::YFP, which showed intense fluorescence at the nucleolus region in the center of the nuclei (71,72) and decreased chromosomal signal (Supplementary Figure S5A). Nucleolar CENP-A^{CID}::YFP local-

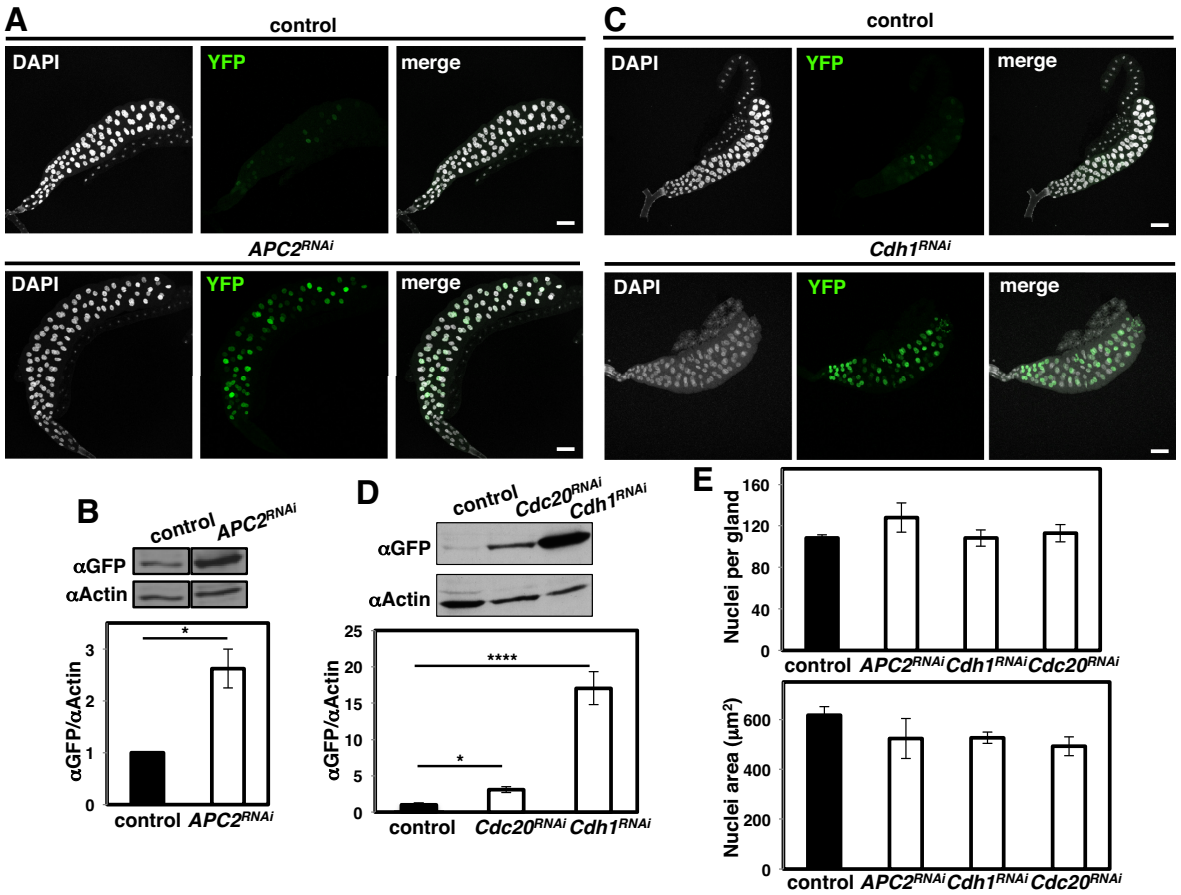

Figure 4. APC/C regulates CENP-A^{CID} expression. (**A**) The expression of CENP-A^{CID}::YFP in salivary glands is determined by direct fluorescence (in green) in control *ey3.5*>CENP-A^{CID}::YFP flies (top) and APC2-depleted *ey3.5*>CENP-A^{CID}::YFP; *APC2^{RNAi}* flies (bottom). DNA was stained with DAPI (in white). Scale bars correspond to 100 μm. (**B**) WB analysis with αGFP antibodies of the levels of CENP-A^{CID}::YFP expression in salivary glands from control *ey3.5*>CENP-A^{CID}::YFP flies and APC2-depleted *ey3.5*>CENP-A^{CID}::YFP; *APC2^{RNAi}* flies. αActin antibodies were used as loading control. Quantitative analysis of the results is shown in the bottom ($N = 2$; **P*-value < 0.01, two-tailed *t*-test; error bars are SEM). (**C**) As in A but for control *ey3.5*>CENP-A^{CID}::YFP flies and Cdh1-depleted *ey3.5*>CENP-A^{CID}::YFP; *Cdh1^{RNAi}* flies. (**D**) As in B but for control *ey3.5*>CENP-A^{CID}::YFP flies, Cdc20-depleted *ey3.5*>CENP-A^{CID}::YFP; *Cdc20^{RNAi}* flies and Cdh1-depleted *ey3.5*>CENP-A^{CID}::YFP; *Cdh1^{RNAi}* flies Quantitative analysis of the results is shown in the bottom ($N \geq 2$; **P* < 0.01, *****P* < 0.00001, two-tailed *t*-test; error bars are SEM). (**E**) In the top, the number of nuclei per gland is presented for control *ey3.5*>CENP-A^{CID}::YFP flies ($N = 10$), APC2-depleted *ey3.5*>CENP-A^{CID}::YFP; *APC2^{RNAi}* flies ($N = 2$), Cdh1-depleted *ey3.5*>CENP-A^{CID}::YFP; *Cdh1^{RNAi}* flies ($N = 8$) and Cdc20-depleted *ey3.5*>CENP-A^{CID}::YFP; *Cdc20^{RNAi}* flies ($N = 4$) (*P*-value > 0.01, two-tailed *t*-test; error bars are SEM). In the bottom, nuclei area of salivary glands cells is presented for control *ey3.5*>CENP-A^{CID}::YFP flies ($N = 10$), APC2-depleted *ey3.5*>CENP-A^{CID}::YFP; *APC2^{RNAi}* flies ($N = 2$), Cdh1-depleted *ey3.5*>CENP-A^{CID}::YFP; *Cdh1^{RNAi}* flies ($N = 8$) and Cdc20-depleted *ey3.5*>CENP-A^{CID}::YFP; *Cdc20^{RNAi}* flies ($N = 4$) (*P*-value > 0.01, two-tailed *t*-test; error bars are SEM).

ization was also observed when Cal1 was overexpressed in Cdh1-depleted and wild type glands (Supplementary Figures S5B and S5C). CENP-A^{CID}::YFP localization at the nucleolus is likely driven by its interaction with Cal1 that is known to localize at the nucleolus in interphase (25,69). Expression of a Cal1::EGFP construct confirmed its nucleolar localization in salivary glands (Supplementary Figure S5D).

Altogether these results suggest that the Cal1-CENP-A^{CID}::YFP complex is resistant to Ppa-mediated degradation, but not to degradation mediated by Cdh1.

DISCUSSION

Here we have shown that CENP-A^{CID} expression is tightly regulated during cell cycle progression through the combined action of SCF^{Ppa} and APC/C^{Cdh1}. In G1, APC/C^{Cdh1} and SCF^{Ppa} regulate CENP-A^{CID} levels, with SCF^{Ppa} acting also in S-phase. The mechanisms regulating CENP-A^{CID} expression in mitosis are less well understood. On one hand, although SCF^{Ppa} is likely present in mitosis, it does not regulate CENP-A^{CID} expression levels. It is possible that Ppa is inactivated or, alternatively, that CENP-A^{CID} is resistant to Ppa-mediated degradation in mitosis (see below). On the other hand, CENP-A^{CID} levels increase upon Cdc20 depletion, suggesting that APC/C^{Cdc20}, which is active in mitosis, regulates CENP-A^{CID} expression. However, despite Cdc20 depletion in the eye imaginal disc induced a strong mitotic arrest, increased CENP-A^{CID} expression was principally detected in non-mitotic cells. In addition, Cdc20 depletion also increased CENP-A^{CID} expression in the endocycling salivary gland cells that do not undergo mitosis.

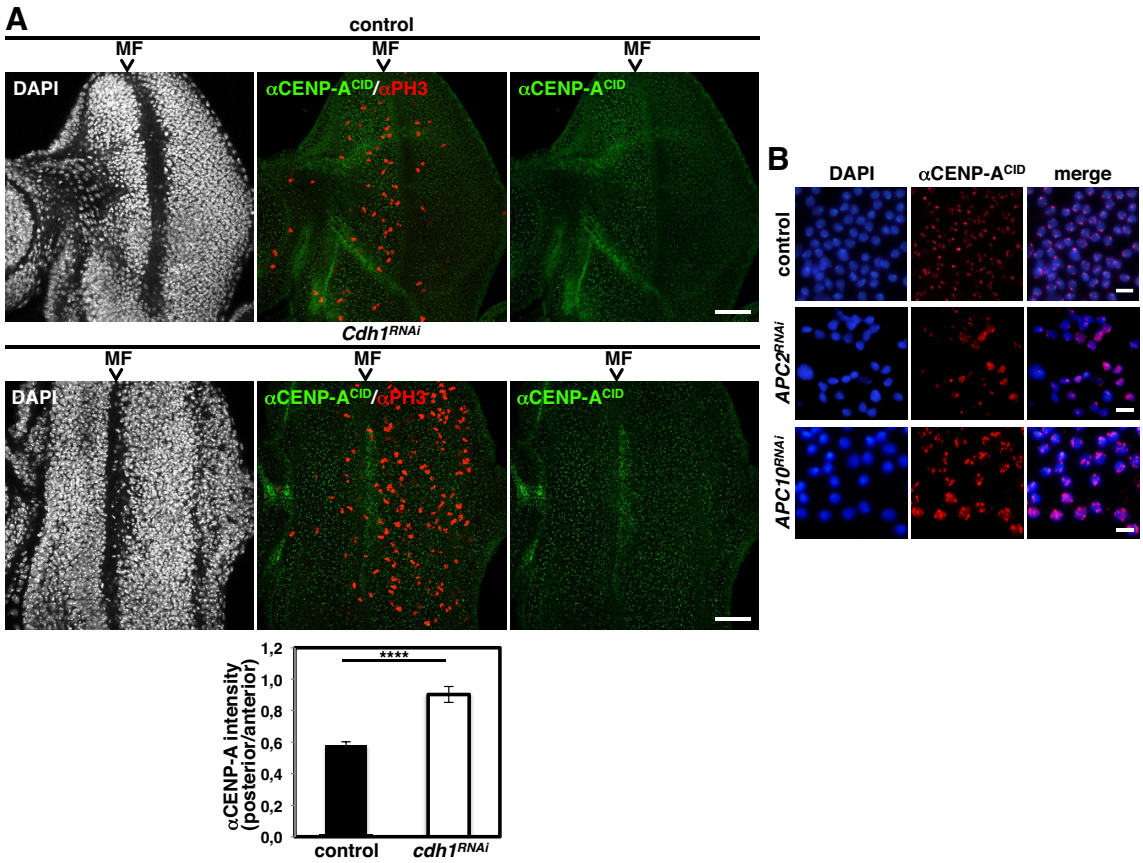

Figure 5. APC/C regulates endogenous CENP-A^{CID} levels. (**A**) Endogenous CENP-A^{CID} expression in the eye imaginal disc is determined by immunostaining with αCENP-A^{CID} (in green) in control *ey3.5* (top) and Cdh1-depleted *ey3.5>Cdh1^{RNAi}* flies (bottom). Immunostainings with αPH3, which marks mitotic cells, are also presented (in red). DNA was stained with DAPI (in white). The position of the MF is indicated. Scale bar corresponds to 25 μm. In the bottom, the integrated intensity of fluorescence in posterior *versus* anterior cells is presented for control *ey3.5* flies ($N = 17$) and Cdh1-depleted *ey3.5>Cdh1^{RNAi}* flies ($N = 13$) (****P-value < 0.0001; two-tailed t-test; errors bars are SEM). (**B**) Immunostaining with αCENP-A^{CID} (in red) of brain squashes from control *elav*-GAL4 (top), APC2-depleted *elav>APC2^{RNAi}* (center) and APC10-depleted *elav>APC10^{RNAi}* larvae (bottom). DNA was stained with DAPI (in blue). Scale bars correspond to 5 μm.

The CENP-A^{CID} specific chaperone Cal1 protects CENP-A^{CID} from Ppa-mediated degradation, but not from degradation induced by Cdh1. These observations suggest a model by which SCF^{Ppa} can degrade only the pool of CENP-A^{CID} that is not in complex with Cal1, whereas APC/C^{Cdh1} can degrade CENP-A^{CID} in the Cal1-CENP-A^{CID} deposition complex. APC/C^{Cdh1} could mediate degradation of the complex itself or, alternatively, of Cal1, rendering CENP-A^{CID} free for degradation by SCF^{Ppa}. Against this second possibility, we observed that endogenous Cal1 levels were not significantly affected upon Cdh1 depletion (Supplementary Figure S6). APC/C^{Cdh1} mediates degradation of CENP-A^{CID} also when it is not in complex with Cal1 since, in Ppa-knockdown conditions, Cal1 depletion did not significantly affect CENP-A^{CID} levels. However, APC/C^{Cdh1} appears to degrade CENP-A^{CID} more efficiently when it is in complex with Cal1 since, upon Cal1 overexpression in Ppa-depleted glands, the levels of CENP-A^{CID} associated with chromosomes were strongly reduced and the remaining CENP-A^{CID} accumulated in the nucleolus, where Cdh1 might not be active. In this regard, Cal1 has been shown to promote CENP-A^{CID} monoubiquitylation by the E3-ligase Cul3/Rdx (73). Thus, it is possible that Cal1 also facilitates CENP-A^{CID} ubiquitylation and degradation by APC/C^{Cdh1}.

SCF^{Ppa} likely regulates CENP-A^{CID} levels directly since Ppa was shown to physically interact with CENP-A^{CID} (57). Whether APC/C^{Cdh1} is directly responsible for CENP-A^{CID} degradation remains to be determined since co-IP experiments failed to detect an interaction between Cdh1 and CENP-A^{CID} or Cal1. Thus, we cannot exclude the possibility that APC/C^{Cdh1} directly targets an unknown positive regulator of CENP-A^{CID} stability different from Cal1. Further work is required to elucidate the precise molecular mechanism of the contribution of APC/C^{Cdh1} to the regulation of CENP-A^{CID} levels.

In somatic tissues of *Drosophila* larvae, centromeric CENP-A^{CID} deposition initiates at late telophase and continues during G1 (13), when APC/C^{Cdh1} is active. Similarly, in S2 cells, deposition occurs starting in mitosis and continuing in G1 (11,14). These observations suggest that APC/C^{Cdh1} activity is important to regulate Cal1-CENP-A^{CID} levels during deposition. On the other hand, SCF^{Ppa} appears especially important to prevent CENP-A^{CID} misin-

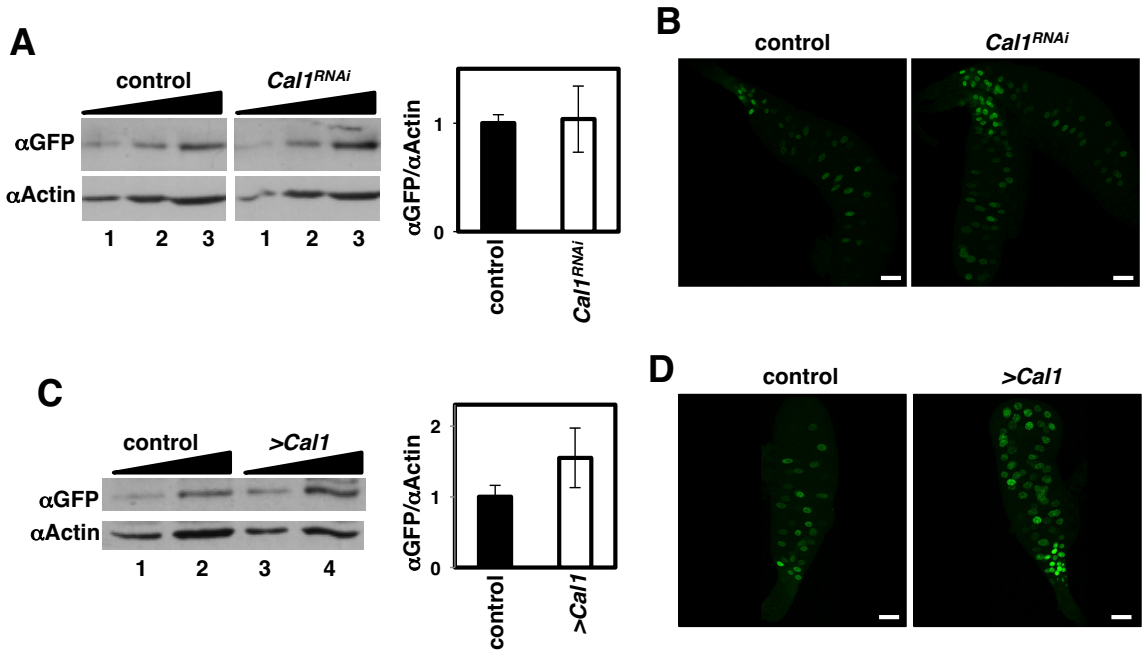

Figure 6. The contribution of Cal1 to CENP-A^{CID} expression. (**A**) WB analysis with αGFP antibodies of the levels of CENP-A^{CID}::YFP expression in salivary glands from control *ey3.5*>CENP-A^{CID}::YFP flies and Cal1-depleted *ey3.5*>CENP-A^{CID}::YFP; *Cal1^{RNAi}* flies. Increasing amounts of extract are analyzed (lanes 1–3). αActin antibodies were used as loading control. Quantitative analysis of the results is shown in the right ($N = 3$; P-value > 0.01, two-tailed t-test; errors bars are SEM). (**B**) The expression of CENP-A^{CID}::YFP in salivary glands is determined by direct fluorescence (in green) in control *ey3.5*>CENP-A^{CID}::YFP flies (left) and Cal1-depleted *ey3.5*>CENP-A^{CID}::YFP; *Cal1^{RNAi}* flies (right). Scale bars correspond to 100 μm. (**C**) As in A but for control *ey3.5*>CENP-A^{CID}::YFP flies and *ey3.5*>CENP-A^{CID}::YFP; UAS-Cal1 flies overexpressing Cal1. (N = 2; P-value>0.01, two-tailed t-test; errors bars are SEM). (**D**) As in B but for control *ey3.5*>CENP-A^{CID}::YFP flies and *ey3.5*>CENP-A^{CID}::YFP; UAS-Cal1 flies overexpressing Cal1. Scale bars correspond to 100 μm.

corporation across chromatin when the bulk of newly synthesized nucleosomes are deposited during DNA replication, as it is active in S-phase when APC/C^{Cdh1} is not. In G1, SCF^{Ppa} could also be instrumental in the degradation of CENP-A^{CID} misincorporated at non-centromeric sites.

Our model predicts that the actual contribution of SCF^{Ppa} and APC/C^{Cdh1} to the regulation of CENP-A^{CID} levels would depend on the actual proportion of total CENP-A^{CID} that is in complex with Cal1, as well as on the relative activities of both enzymes, thus likely varying between cell types and conditions. This means that the effect of Ppa depletion would depend on the amount of CENP-A^{CID} that is not in complex with Cal1, being less important when the Cal1-CENP-A^{CID} complex is more abundant during mitosis, which might account for the lack of effect observed in mitosis. Along the same lines, the effects of Cal1 depletion would depend on the relative abundance of the Cal1-CENP-A^{CID} complex and the activity of Cdh1. In this regard, endocycling cells, such as those of salivary glands, have very high Cdh1 activity that, together with the overexpression of CENP-A^{CID}, suggest that the proportion of Cal1-CENP-A^{CID} in our experiments must be lower than in other experiments performed in cell types with normal Cdh1 activity and no CENP-A^{CID} overexpression, likely accounting for the different effects of Cal1 depletion observed with respect to experiments performed in S2 cells (25,27). Our model also accounts for the stronger effect of Cdh1 depletion in comparison to Ppa depletion since Cdh1 mediates degradation of CENP-A^{CID} regardless of whether it is in complex with Cal1 or not, whereas Ppa only targets the subset that is not in complex with Cal1. In addition, the extent of Ppa knockdown achieved in our experiments was relatively low, as total *ppa* mRNA levels were reduced by only ∼1/3 (57).

A necrotic eye phenotype was observed when CENP-A^{CID} expression was driven by long*GMR*-GAL4 in the most posterior undifferentiated cells of the eye imaginal disc. This phenotype was associated with CENP-A^{CID} overexpression since it was highly enhanced by simultaneous Ppa depletion, which strongly increased CENP-A^{CID} levels and induced its mislocalization across chromatin. In budding yeast, blocking CENP-A^{Cse4} proteolysis leads to its mislocalization and preferential deposition at promoters, resulting in strong changes in gene expression (42). Therefore, preventing CENP-A^{CID} proteolysis could also lead to its preferential deposition at promoters, affect gene expression and, ultimately, interfere with cell differentiation and cause necrosis.

From these studies, proteolysis emerges as a major mechanism regulating CENP-A^{CID} levels. In this regard, regulation at the transcriptional level appears to play a less important role since expression of a CENP-A^{CID}::GFP transgene driven by the endogenous CENP-A^{CID} promoter was detected all across the cell cycle (11). Finally, CENP-A is found overexpressed in various cancers and elevated CENP-A levels correlate with the most aggressive cases (40,41,44,47–52). To what extent, the increased CENP-A content of cancer cells reflects misregulation of the prote-

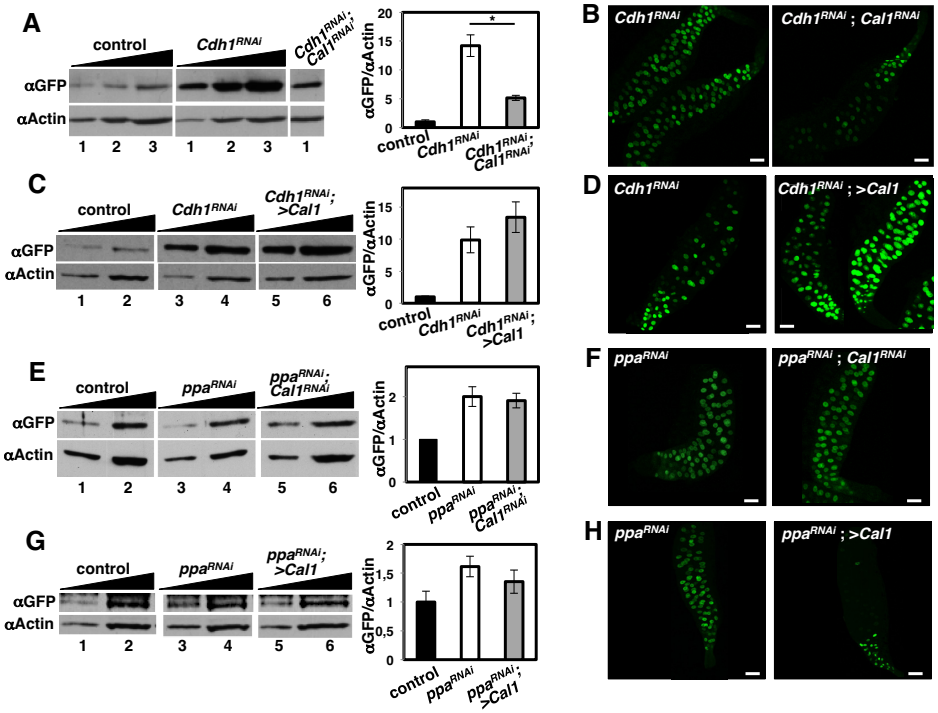

Figure 7. Cal 1 protects CENP-A^{CID} from Ppa-mediated degradation. (**A**) WB analysis with αGFP antibodies of the levels of CENP-A^{CID}::YFP expression in salivary glands from control *ey3.5*>CENP-A^{CID}::YFP flies, Cdh1-depleted *ey3.5*>CENP-A^{CID}::YFP; *Cdh1^{RNAi}* flies and double Cdh1+Cal1-depleted *ey3.5*>CENP-A^{CID}::YFP; *Cdh1^{RNAi}*; *Cal1^{RNAi}* flies. Increasing amounts of extract are analyzed (lanes 1–3). Quantitative analysis of the results is shown in the right ($N \geq 2$; *P-value <0.01; error bars are SEM). (**B**) The expression of CENP-A^{CID}::YFP in salivary glands is determined by direct fluorescence (in green) in Cdh1-depleted *ey3.5*>CENP-A^{CID}::YFP; *Cdh1^{RNAi}* flies and double Cdh1+Cal1-depleted *ey3.5*>CENP-A^{CID}::YFP; *Cdh1^{RNAi}*; *Cal1^{RNAi}* flies. Scale bars correspond to 100 μm. (**C**) As in A but for control *ey3.5*>CENP-A^{CID}::YFP flies, Cdh1-depleted *ey3.5*>CENP-A^{CID}::YFP; *Cdh1^{RNAi}* flies and Cdh1-depleted *ey3.5*>CENP-A^{CID}::YFP; *Cdh1^{RNAi};* UAS-Cal1 flies overexpressing Cal1 ($N = 3$; P-value > 0.01, two-tailed t-test; errors bars are SEM). (**D**) As in B but for Cdh1-depleted *ey3.5*>CENP-A^{CID}::YFP; *Cdh1^{RNAi}* flies and Cdh1-depleted *ey3.5*>CENP-A^{CID}::YFP; *Cdh1^{RNAi};* UAS-Cal1 flies overexpressing Cal1. For the later, two examples are presented with the gland in the right showing increased CENP-A^{CID}::YFP expression. Scale bars correspond to 100 μm. (**E**) As in A but for control *ey3.5*>CENP-A^{CID}::YFP flies, Ppa-depleted *ey3.5*>CENP-A^{CID}::YFP; *ppa^{RNAi}* flies and double Ppa+Cal1-depleted *ey3.5*>CENP-A^{CID}::YFP; *ppa^{RNAi}*; *Cal1^{RNAi}* flies ($N = 2$; P-value > 0.01, two-tailed t-test; errors bars are SEM). (**F**) As in B but for Ppa-depleted *ey3.5*>CENP-A^{CID}::YFP; *ppa^{RNAi}* flies and double Ppa+Cal1-depleted *ey3.5*>CENP-A^{CID}::YFP; *ppa^{RNAi}*; *Cal1^{RNAi}* flies. Scale bars correspond to 100 μm. (**G**) As in A but for control *ey3.5*>CENP-A^{CID}::YFP flies, Ppa-depleted *ey3.5*>CENP-A^{CID}::YFP; *ppa^{RNAi}* flies and Ppa-depleted *ey3.5*>CENP-A^{CID}::YFP; *ppa^{RNAi};* UAS-Cal1 flies overexpressing Cal1 ($N = 2$; P-value > 0.01, two-tailed t-test; errors bars are SEM). (**H**) As in B but for Ppa-depleted *ey3.5*>CENP-A^{CID}::YFP; *ppa^{RNAi}* flies and Ppa-depleted *ey3.5*>CENP-A^{CID}::YFP; *ppa^{RNAi};* UAS-Cal1 flies overexpressing Cal1. Scale bars correspond to 100 μm.

olytic pathways that regulate CENP-A stability remains to be determined.

SUPPLEMENTARY DATA

Supplementary Data are available at NAR Online.

ACKNOWLEDGEMENTS

We are thankful to Drs Aaron F. Straight, Sylvia Erhardt, Christian Lehner, Jordan Raff, Yuu Kimata and Maria Lluisa Espinás for materials. We also acknowledge the help of E. Orsi in related experiments.

FUNDING

MINECO [BFU2015-65082-P]; Generalitat de Catalunya [SGR2014-204, SGR2017-475]; European Community FEDER program; 'Centre de Referència en Biotecnologia' of the Generalitat de Catalunya. Funding for open access charge: MINECO [BFU2015-65082-P]; Generalitat de Catalunya [SGR2014-204, SGR2017-475]; European Community FEDER program.
Conflict of interest statement. None declared.

REFERENCES

1. Allshire,R.C. and Karpen,G.H. (2008) Epigenetic regulation of centromeric chromatin: old dogs, new tricks? *Nat. Rev. Genet.*, **9**, 923–937.
2. Black,B.E. and Cleveland,D.W. (2011) Epigenetic centromere propagation and the nature of CENP-A nucleosomes. *Cell*, **144**, 471–479.
3. Maddox,P.S., Corbett,K.D. and Desai,A. (2012) Structure, assembly and reading of centromeric chromatin. *Curr. Opin. Genet. Dev.*, **22**, 139–147.
4. Malik,H.S. and Henikoff,S. (2009) Major evolutionay transitions in centromere complexity. *Cell*, **138**, 1067–1082.
5. Torras-Llort,M., Moreno-Moreno,O. and Azorín,F. (2009) Focus on the centre: the role of chromatin on the regulation of centromere identity and function. *EMBO J.*, **28**, 2337–2348.
6. McKinley,K.L. and Cheeseman,I.M. (2016) The molecular basis for centromere identity and function. *Nat. Rev. Mol. Cell Biol.*, **17**, 16–29.
7. Ahmad,K. and Henikoff,S. (2001) Centromeres are specilized replication domains in heterochromatin. *J. Cell Biol.*, **153**, 101–110.

8. Shelby,R.D., Monier,K. and Sullivan,K.F. (2000) Chromatin assembly at kinetochores is uncoupled from DNA replication. *J. Cell Biol.*, **151**, 1113–1118.
9. Hemmerich,P., Weidtkamp-Peters,S., Hoischen,C., Schmiedeberg,L., Erliandri,I. and Diekmann,S. (2008) Dynamics of inner kinetochore assembly and maintenance in living cells. *J. Cell Biol.*, **180**, 1101–1114.
10. Jansen,L.E.T., Black,B.E., Foltz,D.R. and Cleveland,D.W. (2007) Propagation of centromeric chromatin requires exit from mitosis. *J. Cell Biol.*, **176**, 795–805.
11. Lidsky,P.V., Sprenger,F. and Lehner,C.F. (2013) Distinct modes of centromere protein dynamics during cell cycle progression in *Drosophila* S2R+ cells. *J. Cell Sci.*, **126**, 4782–4793.
12. Schuh,M., Lehner,C.F. and Heidmann,S. (2007) Incorporation of *Drosophila* CID/CENP-A and CENP-C into centromeres during early embryonic anaphase. *Curr. Biol.*, **17**, 237–243.
13. Dunleavy,E.M., Beier,N.L., Gorgescu,W., Tang,J., Costes,S.V. and Karpen,G.H. (2012) The cell cycle timing of centromeric chromatin assembly in *Drosophila* meiosis is distinct from mitosis yet requires CAL1 and CENP-C. *PLoS Biol.*, **10**, e1001460.
14. Mellone,B.G., Grive,K.J., Shteyn,V., Bowers,S.R., Oderberg,I. and Karpen,G.H. (2011) Assembly of *Drosophila* centromeric chromatin proteins during mitosis. *PLoS Genet.*, **7**, e1002068.
15. Fujita,Y., Hayashi,T., Kiyomitsu,T., Toyoda,Y., Kokubu,A., Obuse,C. and Yanagida,M. (2007) Priming of centromere for CENP-A recruitment by human hMis18alpha, hMis18beta, and M18BP1. *Dev. Cell*, **12**, 17–30.
16. Hayashi,T., Fujita,Y., Iwasaki,O., Adachi,Y., Takahashi,K. and Yanagida,M. (2004) Mis16 and Mis18 are required for CENP-A loading and histone deacetylation at centromeres. *Cell*, **118**, 715–729.
17. Maddox,P.S., Hyndman,F., Monen,J., Oegama,K. and Desai,A. (2007) Functional genomics identifies a Myb domain-containing protein family required for assembly of CENP-A chromatin. *J. Cell Biol.*, **176**, 757–763.
18. French,B.T., Westhorpe,F.G., Limouse,C. and Straight,A.F. (2017) *Xenopus laevis* M18BP1 directly binds existing CENP-A nucleosomes to promote centromeric chromatin assembly. *Dev. Cell*, **42**, 190–199.
19. Hori,T., Shang,W.H., Hara,M., Ariyoshi,M., Arimura,Y., Fujita,R., Kurumizaka,H. and Fukagawa,T. (2017) Association of M18BP1/KNL2 with CENP-A nucleosome is essential for centromere formation in non-mammalian vertebrates. *Dev. Cell*, **42**, 181–189.
20. Camahort,R., Li,B., Florens,L., Swanson,S.K. and Washburn,M.P. (2007) Scm3 is essential to recruit the histone H3 variant CSE4 to centromeres and to maintain a functional kinetochore. *Mol. Cell*, **26**, 853–865.
21. Mizuguchi,G., Xiao,H., Wisniewski,J., Smith,M.M. and Wu,C. (2007) Nonhistone Scm3 and histones CenH3-H4 assemble the core of centromere-specific nucleosomes. *Cell*, **129**, 1153–1164.
22. Pidoux,A.L., Choi,E.S., Abbott,J.K.R., Liu,X., Kagansky,A., Castillo,A.G., Hamilton,G.L., Richardson,W., Rappsilber,J., He,X. *et al.* (2009) Fission yeast Scm3: a CENP-A receptor required for integrity of subkinetochore chromatin. *Mol. Cell*, **33**, 299–311.
23. Phansalkar,R., Lapierre,P. and Mellone,B.G. (2012) Evolutionary insights into the role of the essential centromere protein CAL1 in *Drosophila*. *Chromosome Res.*, **20**, 493–504.
24. Schittenhelm,R.B., Althoff,F., Heidmann,S. and Lehner,C.F. (2010) Detrimental incorporation of excess Cenp-A/Cid and Cenp-C into *Drosophila* centromeres is prevented by limiting amounts of the bridging factor Cal1. *J. Cell Sci.*, **123**, 3768–3779.
25. Erhardt,S., Mellone,B.G., Betts,C.M., Zhang,W., Karpen,G.H. and Straight,A.F. (2008) Genome-wide analysis reveals a cell cycle-dependent mechanism controlling centromere propagation. *J. Cell Biol.*, **183**, 805–818.
26. Goshima,G., Wollman,R., Goodwin,S.S., Zhang,N., Scholey,J.M., Vale,R.D. and Stuurman,N. (2007) Genes required for mitotic spindle assembly in *Drosophila* S2 cells. *Science*, **316**, 417–421.
27. Chen,C.C., Dechassa,M.L., Bettini,E., Ledoux,M.B., Belisario,C., Heun,P., Luger,K. and Mellone,B.G. (2014) CAL1 is the *Drosophila* CENP-A assembly factor. *J. Cell Biol.*, **204**, 313–329.
28. Rosin,L. and Mellone,B.G. (2016) Co-evolving CENP-A and CAL1 domains mediate centromeric CENP-A deposition across *Drosophila* species. *Dev. Cell*, **37**, 136–147.
29. Dunleavy,E.M., Roche,D., Tagami,H., Lacoste,N., Ray-Gallet,D., Nakamura,Y., Daigo,Y., Nakatani,Y. and Almouzni-Pettinotti,G. (2009) HJURP is a cell cycle dependent maintenance and deposition factor of CENP-A at centromeres. *Cell*, **137**, 485–497.
30. Foltz,D.R., Jansen,L.E.T., Bailey,A.O., Yates,J.R. III, Bassett,E.A., Wood,S., Black,B.E. and Cleveland,D.W. (2009) Centromere specific assembly of CENP-A nucleosomes is mediated by HJURP. *Cell*, **137**, 472–484.
31. Bernad,R., Sánchez,P., Rivera,T., Rodríguez-Corsino,M., Boyarchuk,E., Vassias,I., Ray-Gallet,D., Arnaoutov,A., Dasso,M., Almouzni,G. *et al.* (2011) Xenopus HJURP and condensin II are required for CENP-A assembly. *J. Cell Biol.*, **192**, 569–582.
32. Stankovic,A., Guo,L.Y., Mata,J.F., Bodor,D.L., Cao,X.J., Bailey,A.O., Shabanowitz,J., Hunt,D.F., Garcia,B.A., Black,B.E. *et al.* (2017) A dual inhibitory mechanism sufficient to maintain cell-cycle-restricted CENP-A assembly. *Mol. Cell*, **65**, 231–246.
33. Choi,E.S., Stralfors,A., Castillo,A.G., Durand-Dubief,M., Ekwall,K. and Allshire,R.C. (2011) Identification of noncoding transcripts from within CENP-A chromatin at fission yeast centromeres. *J. Biol. Chem.*, **286**, 23600–23607.
34. Choi,E.S., Stralfors,A., Catania,S., Castillo,A.G., Svensson,J.P., Pidoux,A.L., Ekwall,K. and Allshire,R.C. (2012) Factors that promote H3 chromatin integrity during transcription prevent promiscuous deposition of CENPA (Cnp1) in fission yeast. *PLoS Genet.*, **8**, e1002985.
35. Collins,K.A., Furuyama,S. and Biggins,S. (2004) Proteolysis contributes to the exclusive centromere localization of the yeast Cse4/CENP-A histone H3 variant. *Curr. Biol.*, **14**, 1968–1972.
36. Gascoigne,K.E., Takeuchi,K., Suzuki,A., Hori,T., Fukagawa,T. and Cheeseman,I.M. (2011) Induced ectopic kinetochore assembly bypasses the requirement for CENP-A nucleosomes. *Cell*, **145**, 410–422.
37. Mendiburo,M.J., Padeken,J., Fülöp,S., Schepers,A. and Heun,P. (2011) *Drosophila* CENH3 is sufficient for centromere formation. *Science*, **334**, 686–690.
38. Moreno-Moreno,O., Torras-Llort,M. and Azorín,F. (2006) Proteolysis restricts localization of CID, the centromere-specific histone H3 variant of *Drosophila*, to centromeres. *Nucleic Acids Res.*, **34**, 6247–6255.
39. Van Hooser,A.A., Ouspenski,I.I., Gregson,H.C., Starr,D.A., Yen,T.J., Goldberg,M.L., Yokomori,K., Earnshaw,W.C., Sullivan,K.F. and Brinkley,B.R. (2001) Specification of kinetochore-forming chromatin by the histone H3 variant CENP-A. *J. Cell Sci.*, **114**, 3529–3542.
40. Athwal,R.K., Walkiewicz,M.P., Baek,S., Fu,S., Bui,M., Camps,J., Ried,T., Sung,M.H. and Dalal,Y. (2015) CENP-A nucleosomes localize to transcription factor hotspots and subtelomeric sites in human cancer cells. *Epigenet. Chromatin*, **8**, 2.
41. Filipescu,D., Naughtin,M., Podsypanina,K., Lejour,V., Wilson,L., Gurard-Levin,Z.A., Orsi,G.A., Simeonova,I., Toufektchan,E., Attardi,L.D. *et al.* (2017) Essential role for centromeric factors following p53 loss and oncogenic transformation. *Genes Dev.*, **31**, 463–480.
42. Hildebrand,E.M. and Biggins,S. (2016) Regulation of budding yeast CENP-A levels prevents misincorporation at promoter nucleosomes and transcriptional defects. *PLoS Genet.*, **12**, e1005930.
43. Lacoste,N., Woolfe,A., Tachiwana,H., Garea,A.V., Barth,T., Cantaloube,S., Kurumizaka,H., Imhof,A. and Almouzni,G. (2014) Mislocalization of the centromeric histone variant CenH3/CENP-A in human cells depends on the chaperone DAXX. *Mol. Cell*, **53**, 631–644.
44. Amato,A., Schillaci,T., Lentini,L. and Di Leonardo,A. (2009) CENPA overexpression promotes genome instability in pRb-depleted human cells. *Mol. Cancer*, **8**, 119.
45. Heun,P., Erhardt,S., Blower,M.D., Weiss,S., Skora,A.D. and Karpen,G.H. (2006) Mislocalization of the *Drosophila* centromere-specific histone CID promotes formation of functional ectopic kinetochores. *Dev. Cell*, **10**, 303–315.
46. Mathew,V., Pauleau,A.L., Steffen,N., Bergner,A., Becker,P.B. and Erhardt,S. (2014) The histone-fold protein CHRAC14 influences chromatin composition in response to DNA damage. *Cell Rep.*, **7**, 321–330.
47. Hu,Z., Huang,G., Sadanandam,A., Gu,S., Lenburg,M.E., Pai,M., Bayani,N., Blakely,E.A., Gray,J.W. and Mao,J.H. (2010) The

expression level of HJURP has an independent prognostic impact and predicts the sensitivity to radiotherapy in breast cancer. *Breast Cancer Res.*, **12**, R18.
48. Li,Y., Zhu,Z., Zhang,S., Yu,D., Yu,H., Liu,L., Cao,X., Wang,L., Gao,H. and Zhu,M. (2011) ShRNA-targeted centromere protein A inhibits hepatocellular carcinoma growth. *PLoS ONE*, **6**, e17794.
49. Ma,X.J., Salunga,R., Tuggle,J.T., Gaudet,J., Enright,E., McQuary,P., Payette,T., Pistone,M., Stecker,K., Zhang,B.M. *et al.* (2003) Gene expression profiles of human breast cancer progression. *Proc. Natl. Acad. Sci. U.S.A.*, **100**, 5974–5979.
50. Qiu,J.J., Guo,J.J., Lv,T.J., Jin,H.Y., Ding,J.X., Feng,W.W., Zhang,Y. and Hua,K.Q. (2013) Prognostic value of centromere protein-A expression in patients with epithelial ovarian cancer. *Tumour Biol.*, **34**, 2971–2975.
51. Tomonaga,T., Matsushita,K., Yamaguchi,S., Oohashi,T., Shimada,H., Ochiai,T., Yoda,K. and Nomura,F. (2003) Overexpression and mistargeting of centromere protein-A in human primary colorectal cancer. *Cancer Res.*, **63**, 3511–3516.
52. Wu,Q., Qian,Y.M., Zhao,X.L., Wang,S.M., Feng,X.J., Chen,X.F. and Zhang,S.H. (2012) Expression and prognostic significance of centromere protein A in human lung adenocarcinoma. *Lung Cancer*, **77**, 407–414.
53. Hewawasam,G., Shivaraju,M., Mattingly,M., Venkatesh,S., Martin-Brown,S., Florens,L., Workman,J.L. and Gerton,J.L. (2010) Psh1 is an E3 ubiquitin ligase that targets the centromeric histone variant Cse4. *Mol. Cell*, **40**, 444–454.
54. Ranjitkar,P., Press,M.O., Yi,X., Baker,R., MacCoss,M.J. and Biggins,S. (2010) An E3 ubiquitin ligase prevents ectopic localization of the centromeric histone H3 variant via the centromere targeting domain. *Mol. Cell*, **40**, 455–464.
55. Cheng,H., Bao,X., Gan,X., Luo,S. and Rao,H. (2017) Multiple E3s promote the degradation of histone H3 variant Cse4. *Sci. Rep.*, **7**, 8565.
56. Ohkuni,K., Takahashi,Y., Fulp,A., Lawrimore,J., Au,W.C., Pasupala,N., Levy-Myers,R., Warren,J., Strunnikov,A., Baker,R.E. *et al.* (2016) SUMO-Targeted Ubiquitin Ligase (STUbL) Slx5 regulates proteolysis of centromeric histone H3 variant Cse4 and prevents its mislocalization to euchromatin. *Mol. Biol. Cell*, **27**, 1500–1510.
57. Moreno-Moreno,O., Medina-Giró,S., Torras-Llort,M. and Azorín,F. (2011) The F box protein partner of paired regulates stability of *Drosophila* centromeric histone H3, CenH3(CID). *Curr. Biol.*, **21**, 1488–1493.
58. Cardozo,T. and Pagano,M. (2004) The SCF ubiquitin ligase: insights into a molecular machine. *Nat. Rev. Mol. Cell Biol.*, **5**, 739–751.
59. Nakayama,K.I. and Nakayama,K. (2006) Ubiquitin ligases: cell-cycle control and cancer. *Nat. Rev. Cancer*, **6**, 369–381.
60. Reed,S.I. (2003) Ratchets and clocks: the cell cycle, ubiquitylation and protein turnover. *Nat. Rev. Mol. Cell Biol.*, **4**, 855–864.
61. Vodermaier,H.C. (2004) APC/C and SCF: controlling each other and the cell cycle. *Curr. Biol.*, **14**, R787–R796.
62. Charlton-Perkins,M., Brown,N.L. and Cook,T.A. (2011) The lens in focus: a comparison of lens development in *Drosophila* and vertebrates. *Mol. Genet. Genomics*, **286**, 189–213.
63. Treisman,J.E. (2013) Retinal differentiation in *Drosophila*. *Wiley Interdiscip. Rev. Dev. Biol.*, **2**, 545–557.
64. Edgar,B.A. and Orr-Weaver,T.L. (2001) Endoreplication cell cycles: more for less. *Cell*, **105**, 297–306.
65. Lee,H.O., Davidson,J.M. and Duronio,R.J. (2009) Endoreplication: polyploidy with purpose. *Genes Dev.*, **23**, 2461–2477.
66. Lilly,M.A. and Duronio,R.J. (2005) New insights into cell cycle control from the *Drosophila* endocycle. *Oncogene*, **24**, 2765–2775.
67. Baker,N.E. (2001) Cell proliferation, survival, and death in the *Drosophila* eye. *Semin. Cell Dev. Biol.*, **12**, 499–507.
68. van Leuken,R., Clijsters,L. and Wolthuis,R. (2008) To cell cycle, swing the APC/C. *Biochim. Biophys. Acta*, **1786**, 49–59.
69. Dawson,I.A., Roth,S., Akam,M. and Artavanis-Tsakonas,S. (1993) Mutations of the *fizzy* locus cause metaphase arrest in *Drosophila melanogaster* embryos. *Development*, **117**, 359–376.
70. Tavormina,P.A. and Burke,D.J. (1998) Cell cycle arrest in cdc20 mutants of *Saccharomyces cerevisiae* is independent of Ndc10p and kinetochore function but requires a subset of spindle checkpoint genes. *Genetics*, **148**, 1701–1713.
71. Vujatovic,O., Zaragoza,K., Vaquero,A., Reina,O., Bernués,J. and Azorín,F. (2012) *Drosophila melanogaster* linker histone dH1 is required for transposon silencing and to preserve genome integrity. *Nucleic Acids Res.*, **40**, 5402–5414.
72. Marinho,J., Casares,F. and Pereira,P.S. (2011) The *Drosophila* Nol12 homologue viriato is a dMyc target that regulates nucleolar architecture and is required for dMyc-stimulated cell growth. *Development*, **138**, 349–357.
73. Bade,D., Pauleau,A.L., Wendler,A. and Erhardt,S. (2014) The E3 ligase CUL3/RDX controls centromere maintenance by ubiquitylating and stabilizing CENP-A in a CAL1-dependent manner. *Dev. Cell*, **28**, 508–519.
74. Krasnow,M.A., Saffman,E.E., Kornfeld,K. and Hogness,D.S. (1989) Transcriptional activation and repression by Ultrabithorax proteins in cultured *Drosophila* cells. *Cell*, **57**, 1031–1043.
75. Schindelin,J., Arganda-Carreras,I., Frise,E., Kaynig,V., Longair,M., Pietzsch,T., Preibisch,S., Rueden,C., Saalfeld,S., Schmid,B. *et al.* (2012) Fiji: an open-source platform for biological-image analysis. *Nat. Methods*, **9**, 676–682.